Key Points:
- We extend a theory of magnetic Rossby waves, which can propagate westward in the Earth's core
- The wave propagation is identified at a correct speed in numerical dynamo simulations
- The rate of the geomagnetic westward drift could reveal the toroidal field strength in the core

Supporting Information:
- Text S1 and Figure S1

Correspondence to:
K. Hori,
amtkh@leeds.ac.uk

Slow magnetic Rossby waves in the Earth's core

K. Hori[1,2], C. A. Jones[1], and R. J. Teed[3]

[1]Department of Applied Mathematics, University of Leeds, Leeds, UK, [2]Solar Terrestrial Environment Laboratory, Nagoya University, Nagoya, Japan, [3]Department of Applied Mathematics and Theoretical Physics, University of Cambridge, Cambridge, UK

Abstract The westward drift component of the secular variation is likely to be a signal of waves riding on a background mean flow. By separating the wave and mean flow contributions, we can infer the strength of the "hidden" azimuthal part of the magnetic field within the core. We explore the origin of the westward drift commonly seen in dynamo simulations and show that it propagates at the speed of the slow magnetic Rossby waves with respect to a mean zonal flow. Our results indicate that such waves could be excited in the Earth's core and that wave propagation may indeed play some role in the longitudinal drift, particularly at higher latitudes where the wave component is relatively strong, the equatorial westward drift being dominated by the mean flow. We discuss a potential inference of the RMS toroidal field strength within the Earth's core from the observed drift rate.

1. Introduction

Magnetohydrodynamic (MHD) waves in a rapidly rotating planetary core can produce secular variations of the magnetic field. Axisymmetric modes are thought to be responsible for the torsional oscillations of cylinders aligned with the rotation axis, which are a type of Alfvén wave, propagating in the cylindrical radial direction along the radial component of magnetic field [*Braginsky*, 1970]. This wave has been found in core flow models inverted from the geomagnetic secular variation, on timescales of several years to decades [*Zatman and Bloxham*, 1997; *Gillet et al.*, 2010] and has also been found in numerical simulations [e.g., *Wicht and Christensen*, 2010; *Teed et al.*, 2014]. By fitting torsional waves to observed field models, several authors have inferred the magnetic field strength in the fluid core [e.g., *Buffett et al.*, 2009] and *Gillet et al.* [2010] deduced a radial field of magnitude 2 mT or larger within the core. Recently, *Buffett* [2014] suggested that axisymmetric MAC waves in a stably stratified layer below the core-mantle boundary could be responsible for the slower, approximately 60 year oscillations seen in the secular variation data.

Most investigations have concentrated on the axisymmetric modes, but there are other waves that can create nonaxisymmetric variations, migrating along the azimuthal magnetic field. These nonaxisymmetric modes may be related to the westward drift of the geomagnetic field, which has been significant in the Atlantic hemisphere for at least the last hundred years [e.g., *Bullard et al.*, 1950; *Yukutake*, 1962; *Bloxham et al.*, 1989; *Finlay and Jackson*, 2003]. These drifts are commonly considered to be due to large-scale zonal flows [e.g., *Bullard et al.*, 1950]. However, propagation of waves may also account for the longitudinal drift. Such waves can be excited in the deep core region [*Hide*, 1966] and possibly in a stably stratified thin layer at the top of the core [*Braginsky*, 1999]. The possibility of waves being important was pointed out in a few studies of the geomagnetic secular variation and core flow inversion [*Holme and Whaler*, 2001; *Jackson*, 2003]. Numerical dynamo simulations without stably stratified layers have successfully reproduced the longitudinal magnetic drift [*Aubert et al.*, 2013]. Some authors reported that the drift rate did not fully match the mean zonal flow speed, suggesting that wave propagation could be at least partly responsible for the drift rate of the magnetic field [e.g., *Kono and Roberts*, 2002; *Christensen and Olson*, 2003]. Even if wave propagation only plays a part in westward drift, by subtracting out the mean flow part, useful information may be gained about the internal toroidal field, which, unlike the poloidal component, is confined within the core and cannot be directly measured outside it.

Nonaxisymmetric oscillations of the core on secular variation timescales are crucially affected by both rotation and magnetic field, and travel in the azimuthal direction [e.g., *Jones*, 2007; *Finlay et al.*, 2010; *Canet et al.*, 2014; *Hori et al.*, 2014]. Rotating MHD waves split into two classes, fast waves where the primary balance is between

inertia and a combination of Coriolis and Lorentz force, and slow waves where inertia is negligible and the core evolves slowly through a sequence of magnetostrophic states. It is these slow waves which are most relevant to current secular variation studies, as the fast waves have periods of only days to months. In general, the slow waves have periods longer than the secular variation timescale, but there is a class of waves, the topographic magnetic Rossby waves (sometimes called Magnetic-Coriolis(MC)-Rossby waves), which do have periods of a few hundred years. This class of waves, derived by *Hide* [1966] in a local β plane model, have the property that the flow is quasi-geostrophic; that is, there is very little variation in the z direction. They propagate westward, and they may be derived as a limit of the full spectrum of global modes for the special case of the Malkus field $\boldsymbol{B} = B_0 s \hat{\boldsymbol{e}}_\phi$ [*Malkus*, 1967; *Canet et al.*, 2014].

In this letter, we extend Hide's theory to the quasi-geostrophic (QG) cylinders and report identification of the slow mode in spherical dynamo simulations. Based on the QG model, we discuss its implications to the geomagnetic secular variation and inferences of the core quantities.

2. Theory

Focusing on waves with timescales of several to hundreds years, which are probably shorter than the diffusion times in the core, we assume that the wave motion is fast enough to ignore the diffusion terms. We also suppose that the magnetic field and flow can be separated into the mean part and fluctuating part; i.e., $\boldsymbol{B} = \widetilde{\boldsymbol{B}} + \boldsymbol{b}'$, $\boldsymbol{u} = \widetilde{\boldsymbol{U}} + \boldsymbol{u}'$, where the mean quantities are temporally averaged. The precise definition of the temporal and spatial averages used are detailed in the supporting information. We consider a balance between inertia, Coriolis and Lorentz forces, and we also assume that the spatial length scale of mean quantities is greater than that of perturbed quantities. We neglect the nonlinear term $\boldsymbol{j}' \times \boldsymbol{b}'$ in comparison with $\boldsymbol{j}' \times \widetilde{\boldsymbol{B}}$, i.e., $|\boldsymbol{b}'| \ll |\widetilde{\boldsymbol{B}}|$, we obtain

$$\rho \frac{\mathrm{d}\boldsymbol{u}'}{\mathrm{d}t} + 2\rho\Omega(\hat{\boldsymbol{e}}_z \times \boldsymbol{u}') = -\nabla p' + \boldsymbol{j}' \times \widetilde{\boldsymbol{B}} , \tag{1}$$

where $\mathrm{d}/\mathrm{d}t = \partial/\partial t + \widetilde{\boldsymbol{U}} \cdot \nabla$, ρ is the density, Ω is the rotational rate, and the electrical current $\boldsymbol{j}' = (\nabla \times \boldsymbol{b}')/\mu_0$ with μ_0 being the magnetic permeability. In the induction equation we also neglect the nonlinear $(\boldsymbol{u}' \cdot \nabla)\boldsymbol{b}'$ in comparison with $(\widetilde{\boldsymbol{U}} \cdot \nabla)\boldsymbol{b}'$ to obtain

$$\frac{\mathrm{d}\boldsymbol{b}'}{\mathrm{d}t} = \widetilde{\boldsymbol{B}} \cdot \nabla \boldsymbol{u}' . \tag{2}$$

Taking the z component of the curl of (1), we obtain the vorticity equation

$$\rho \frac{\mathrm{d}\xi_z'}{\mathrm{d}t} - 2\rho\Omega \frac{\partial u_z'}{\partial z} = \hat{\boldsymbol{e}}_z \cdot \nabla \times (\boldsymbol{j}' \times \widetilde{\boldsymbol{B}}) \tag{3}$$

where $\xi' = \nabla \times \boldsymbol{u}'$ is the vorticity and the mean flow is assumed to have negligible vorticity. Magnetic Rossby waves are quasi-geostrophic [*Hide*, 1966]. A typical snapshot of a meridional slice of u_s' in our simulations is shown in Figure S1 in the supporting information. It has an approximately columnar structure. We therefore make the quasi-geostrophic assumption that u_s' and ξ_z' are independent of z. We integrate (3) over z, from $z = -H$ to H (where $H = \sqrt{r_o^2 - s^2}$), and perform the integral of the second term on the left-hand side by using the sloping boundary conditions $u_z' = \mp u_s' s/H$ at $z = \pm H$, leaving

$$\rho \frac{\mathrm{d}}{\mathrm{d}t} \frac{1}{2H} \int_{-H}^{+H} \xi_z' \mathrm{d}z + \frac{2\rho\Omega s\, u_s'}{r_o^2 - s^2} = \frac{1}{2H} \int_{-H}^{+H} \widetilde{\boldsymbol{B}} \cdot \nabla j_z' \mathrm{d}z . \tag{4}$$

When the azimuthal components of the mean quantities, $\widetilde{\boldsymbol{B}}$ and $\widetilde{\boldsymbol{U}}$, are taken into account and are independent of ϕ and t, substitution of the curl of (2) into the time derivative of (4) gives

$$\frac{\mathrm{d}}{\mathrm{d}t} \left[\frac{\mathrm{d}}{\mathrm{d}t} \frac{1}{2H} \int_{-H}^{+H} \xi_z' \mathrm{d}z + \frac{2\Omega s u_s'}{r_o^2 - s^2} \right] = \frac{1}{2\rho\mu_0 H} \int_{-H}^{+H} \frac{\overline{B_\phi^2}}{s^2} \frac{\partial^2 \xi_z'}{\partial \phi^2} \mathrm{d}z , \tag{5}$$

where $\bar{\ }$ represents an axisymmetric quantity and $\mathrm{d}/\mathrm{d}t = \partial/\partial t + (\overline{\widetilde{U}_\phi}/s)\partial/\partial\phi$. In our simulations, the radial gradient of the velocity is typically smaller than the azimuthal one, and in this case $\xi_z' \approx -(1/s)(\partial u_s'/\partial\phi)$. This

leads to a considerable simplification of the dispersion relation, so we adopt it here, but we note that in other simulations at different parameters this assumption may not be valid. Then (5) becomes

$$\frac{\mathrm{d}}{\mathrm{d}t}\left[\frac{\mathrm{d}}{\mathrm{d}t}\frac{1}{2H}\int_{-H}^{+H}\frac{1}{s}\frac{\partial u_s'}{\partial\phi}\mathrm{d}z - \frac{2\Omega s\,u_s'}{r_o^2-s^2}\right] = \frac{1}{2\rho\mu_0 H}\int_{-H}^{+H}\frac{\overline{B_\phi^2}}{s^3}\frac{\partial^3 u_s'}{\partial\phi^3}\mathrm{d}z \ . \tag{6}$$

Seeking the solution advected by the mean geostrophic flow, i.e., $\boldsymbol{u} \sim s\tilde{\zeta}(s)\hat{\boldsymbol{e}}_\phi + \boldsymbol{u}'(s,\phi,t)$, with a form of $\exp\{i(m\phi - \omega t)\}$, equation (6) can be rewritten as

$$\hat{\omega}\left[\hat{\omega}\frac{m}{s} - \frac{2\Omega s}{r_o^2-s^2}\right]u_s' = \frac{1}{2\rho\mu_0 H}\frac{m^3}{s^3}u_s'\int_{-H}^{+H}\overline{B_\phi^2}\,\mathrm{d}z \ , \tag{7}$$

where $\hat{\omega} = \omega - \tilde{\zeta}m$. This results in a general dispersion relation

$$\hat{\omega}\left[\hat{\omega} - \frac{2\Omega s^2}{(r_o^2-s^2)m}\right] = \frac{1}{\rho\mu_0}\frac{m^2}{s^2}\langle\overline{B_\phi^2}\rangle \ , \tag{8}$$

where $\langle\cdot\rangle$ denotes the z-averaged quantities, yielding the solutions

$$\hat{\omega}_\pm = \omega_\pm - \tilde{\zeta}m = \omega_\beta\left[\frac{1}{2} \pm \frac{1}{2}\sqrt{1 + 4\frac{\omega_M^2}{\omega_\beta^2}}\right] \ , \tag{9}$$

where the Rossby and Alfvén frequencies are

$$\omega_\beta = \frac{2\Omega s^2}{(r_o^2-s^2)m} \quad \text{and} \quad \omega_M^2 = \frac{m^2}{\rho\mu_0}\frac{\langle\overline{B_\phi^2}\rangle}{s^2} \ , \tag{10}$$

respectively. When $\omega_M^2 \gg \omega_\beta^2$, equation (9) is reduced to the Alfvén waves, which travel along the azimuthal field and are nondispersive. On the other hand, when $\omega_M^2 \ll \omega_\beta^2$, they become $\hat{\omega}_+ \approx +\omega_\beta(1 + \omega_M^2/\omega_\beta^2)$ and $\hat{\omega}_- \approx -\omega_M^2/\omega_\beta$. These are essentially the fast and slow modes of magnetic Rossby waves, derived by *Hide* [1966].

The slow mode, which would be of more interest for geophysical applications, is given as

$$\hat{\omega}_{\mathrm{MC}} \equiv -\frac{\omega_M^2}{\omega_\beta} = -\frac{m^3(r_o^2-s^2)\langle\overline{B_\phi^2}\rangle}{2\rho\mu_0\Omega\,s^4} \ . \tag{11}$$

This mode travels westward at a speed slower than the Alfvén mode and is dispersive. With core quantities $(\rho, \Omega, r_\circ)$ being fixed, the frequency depends on m and s, as $\langle\overline{B_\phi^2}\rangle$ is a function of s. Note that the Coriolis term, or the Rossby mode ω_β, goes singular, and the QG approximation certainly breaks down as s is increased toward the core surface $r_\circ$. This means that we cannot use QG theory to explain the westward drift near the equator. As the boundary slope increases as the equator is approached, we expect the magnetic Rossby waves to be slow near the equator, and so the wave components will make only a small contribution to the westward drift compared to the mean flow. It is, however, quite possible for the magnetic Rossby modes to contribute to any longitudinal drifts at higher latitudes, i.e., smaller s, and this is found in the simulations.

3. Numerical Simulation

To explore the magnetic Rossby wave in Earth's core-like situations, we numerically model convection and magnetic field generation in a rotating spherical shell filled with an electrically conducting fluid. We chose runs where torsional oscillations were identified in previous work [*Teed et al.*, 2014]. The model parameters explored in this study are listed in Table 1, where values of the Ekman E and magnetic Prandtl numbers Pm are varied. A detailed description of the model is given in the supporting information. The time intervals τ analyzed are much shorter than the diffusion time, suggesting that inviscid theory can be valid here. We focus on the fluid motion outside the tangent cylinder where the QG approximation is relevant [*Gillet and Jones*, 2006].

Table 1. Simulation Results[a]

						at $s = 0.77r_o$			
Run	E	Pm	Λ	Le	τ	τ^E (years)	$m:V_{MC}$	$m:V_{MC}$	$\tilde{\zeta}$	$B_{T/P}$
4R5	10^{-4}	5	18.2	0.02	0.015	17.7	$5:-123$	$3:-44.1$	-57.9	8.77
5R2	10^{-5}	2	1.78	0.003	0.01	5.77	$9:-23.9$	$13:-49.8$	-34.0	15.3
5R5	10^{-5}	5	21.7	0.007	0.006	30.0	$6:-131$	$4:-58.2$	-107	4.35
6.5R2	5×10^{-6}	2	2.26	0.002	0.01	8.90	$15:-64.4$	$10:-28.6$	-37.6	9.43
6.5R5	5×10^{-6}	5	22.2	0.005	0.004	39.3	$6:-89.5$	$10:-249$	-150	12.8

[a]At Prandtl number $Pr = 1$ and Rayleigh number $Ra = 8.32Ra_c$ with Ra_c being the critical value for the onset of the nonmagnetic convection. See supporting information for the detailed description. The columns Λ, Le, τ, and τ^E list the Elsasser number, the Lehnert number, the analyzed period of time, and the dimensional version of the period (represented in years), respectively. On the right, the values at $r = 0.77r_o$ are shown. At each run the two most dominant wave numbers m and the speeds of the slow magnetic Rossby mode V_{MC} are listed. The relative strength of the internal azimuthal field to the surface radial field is measured by $B_{T/P}$.

To identify the wave motion, we first evaluate the wave speed expected from the theory, given by equation (11). Figure 1a plots the phase speed of the slow magnetic Rossby mode, $V_{MC} = |\hat{\omega}_{MC}/m|$, as a function of the cylindrical radius s, for the run 5R5, using the nondimensional form of (11), with the azimuthal field obtained in the simulation. Here the field $\langle \widetilde{B_\phi^2} \rangle$ is averaged in ϕ, z and time, where $\overline{\cdot}$, $\langle \cdot \rangle$, and $\widetilde{\cdot}$ denote averaging over ϕ, z, and time, respectively. Though the azimuthal field is stronger near the equator, which is reflected in the Alfvén speed, the slow wave propagates faster as the radius is decreased to the inner boundary, as noted in section 2. Since the wave motion will be advected with respect to the background flow, we display in Figure 1b the speed of the axisymmetric azimuthal flow in terms of the angular velocity, $\tilde{\zeta} = \langle \widetilde{u_\phi} \rangle / s$. The flow is generally slower than the expected wave speed, suggesting that the wave motion can be relevant in the run, as long as the excited azimuthal wave number is not too small. For spectral analyses, the advection effect due to this background flow gives a linear dispersion relation, $\omega = \tilde{\zeta}m \equiv \hat{\omega}_{adv}$.
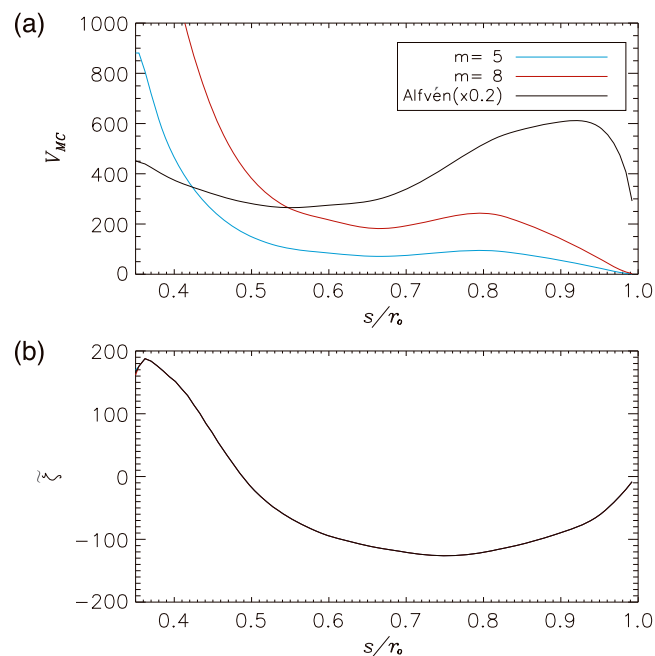
Figure 1. (a) Phase speed of the slow magnetic Rossby wave, $V_{MC} = |\widetilde{\hat{\omega}}_{MC}/m|$, and of the Alfvén wave, $V_A = |\omega_M/m|$, for the run 5R5, which are calculated with the simulation output $\langle \widetilde{B_\phi^2} \rangle$. The Alfvén speed is plotted by multiplying 0.2. (b) Angular velocity $\tilde{\zeta}$ of the axisymmetric azimuthal flow, calculated with $\langle \widetilde{u_\phi} \rangle$.
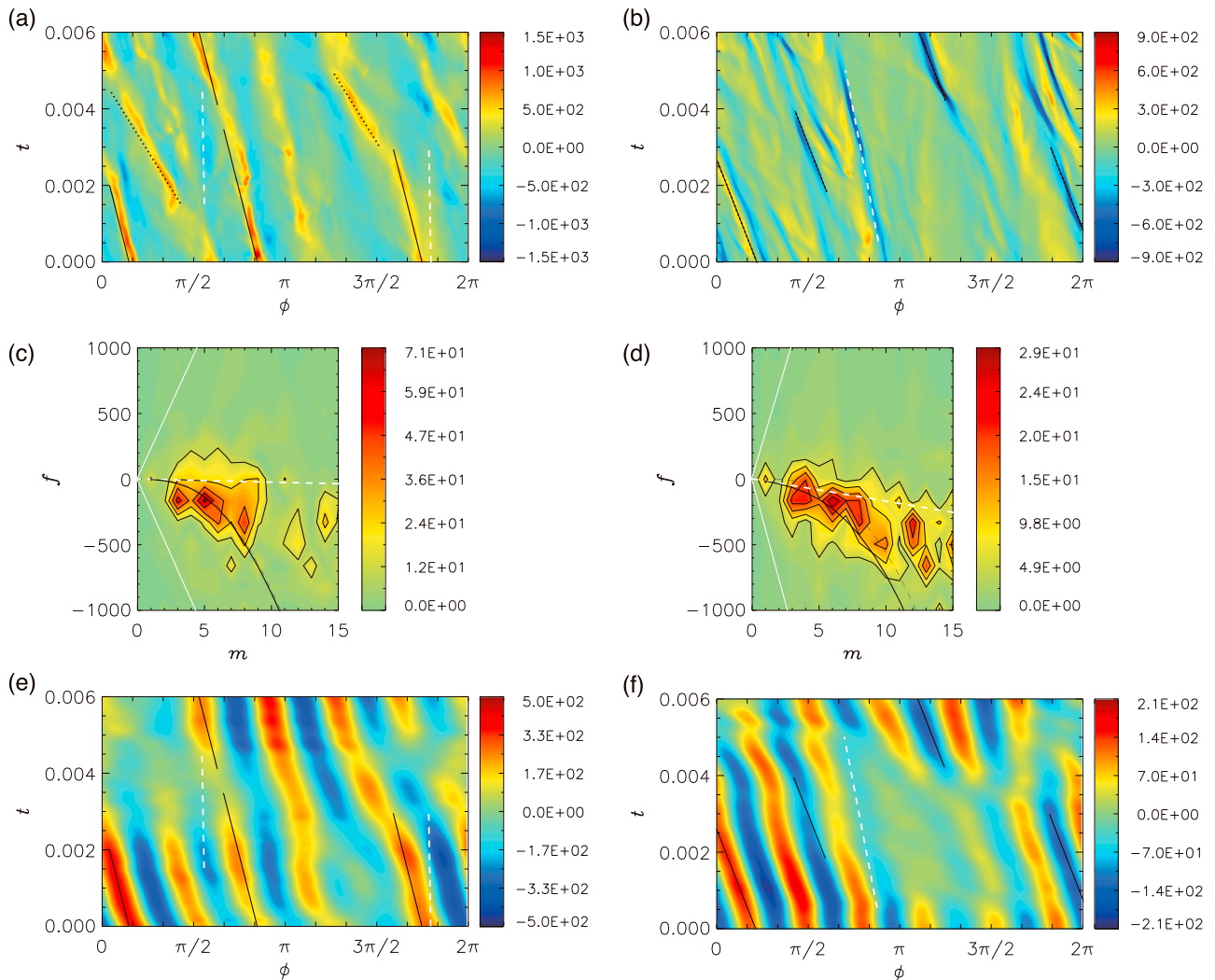
Figure 2. Azimuth time section of $\langle u'_s \rangle$ at (a) $s = 0.5r_\circ$ and (b) $0.77r_\circ$ for the run 5R5. White and black lines represent the advective speed due to the mean zonal flow ($\bar{\zeta}$), and the total speed for the slow magnetic Rossby mode ($\bar{\zeta} + \hat{\omega}_{MC}/m$) with different wave numbers m, respectively, at the radii: $m = 5$ (solid) and 8 (dashed) in Figure 2a and $m = 6$ (solid) in Figure 2b. (c and d) Wave number-frequency power spectrum at the same radii. Here white dashed, black dashed, and black solid lines show the advective dispersion relation, $\hat{\omega}_{adv}/2\pi = \bar{\zeta}m/2\pi$, the slow wave ones, $\hat{\omega}_-/2\pi$ (equation (9)), and the total ones, $(\hat{\omega}_{adv} + \hat{\omega}_-)/2\pi$, respectively. The fast mode, $(\hat{\omega}_{adv} + \hat{\omega}_+)/2\pi$, is far beyond the frequency window here. As m is increased, the modes recover the Alfvén waves, whose dispersion relations, $(\hat{\omega}_{adv} \pm \hat{\omega}_M)/2\pi$, are represented by white solid lines. At sufficiently large m, the black solid curve becomes parallel to the white solid line. (e and f) Same as Figures 2a and 2b, but all the wave numbers are filtered out except $m = 4$ to 6 in Figure 2e and $m = 5$ to 7 in Figure 2f.

Figures 2a and 2b show time azimuthal sections of the z-averaged radial velocity $\langle u'_s \rangle$ at $s = 0.5r_\circ$ and $0.77r_\circ$, for the same run 5R5. Here $'$ denotes the fluctuating part, in which the time-averaged part is removed from the quantity. We find significant westward drifts at both radii. The westward moving features in Figures 2a and 2b are quite narrow, suggesting that the nonlinear terms, omitted in our simple theory, may be significant in our simulations. However, here we concentrate on the linear aspects of the propagating waves. To explore the spectral structure, we perform two-dimensional fast Fourier transformation on the data. The calculated frequency-wave number spectrum is shown in Figures 2c and 2d, where the horizontal axis represents the azimuthal wave number m and the vertical axis the frequency $f = \omega/2\pi$ with the positive (negative) sign representing the prograde (retrograde) drift. Retrograde azimuthal wave numbers in the range 3 to 12 dominate.

We note that $m = 5$ and $m = 8$ give significant contributions in Figure 2c and $m = 6$ in Figure 2d, so we look for features in the azimuthal flow that travel at the wave speeds expected for these modes. In Figures 2a and 2b we added lines to help identify these features. White dashed lines have slope corresponding to the advection speed. This is slow at $s = 0.5r_\circ$ because at this latitude the mean zonal flow changes between

eastward and westward, but some features traveling at the advection speed can be seen at $s = 0.77r_\circ$, latitude 40°. Solid black lines and black dashed lines in Figure 2a correspond to $m = 5$ and $m = 8$, respectively; the slopes corresponding to the total phase speed $(\hat{\omega}_{adv} + \hat{\omega}_{MC})/m$. It is clear that there are features traveling at these wave speeds, showing that there are magnetic Rossby waves in our simulations. In Figure 2b we show the same solid black lines corresponding to the total phase speed with $m = 6$. Figures 2e and 2f are the same as Figures 2a and 2b, except that for $s = 0.5r_\circ$, modes outside the range $m = 4$ to 6 are filtered out, and at $s = 0.77r_\circ$, modes outside the range $m = 5$ to 7 are removed. Note that the filtering makes the magnetic Rossby waves even more evident. The mode gradually transitions to the Alfvén mode as m gets large as can be seen in Figures 2c and 2d.

In Figures 2c and 2d the white dashed lines correspond to the dispersion relation of the advection process, the phase velocity being equal to the zonal flow speed. The dashed black lines give the dispersion relation of magnetic Rossby waves on a stationary fluid, and the solid black lines give the dispersion relation on fluid moving with the zonal flow, so the phase velocity of the solid black line corresponds to the sum of the phase velocities of the two dashed curves.

We learn from Figure 2 that for these parameters the wave speed exceeds the advection speed at latitudes above ±40°, but closer to the equator the magnetic Rossby wave, speed decreases below the advection speed, making it more difficult to separate the wave component from the advection component.

We evaluated the magnitude of the terms in (4) in our simulations. For the run 5R5 we found that the Coriolis and Lorentz forces are approximately in balance, and the inertial term is smaller; the balance expected of a magnetic Rossby wave. We can also rule out the possibility of the waves in Figures 2a and 2b being nonmagnetic Rossby waves, whose phase speed (eastward) and group speed (westward) are approximately 25 times larger than those shown in the these figures.

Table 1 summarizes the simulations we investigated and their output values. We were able to identify the slow wave in each run, although the dominant wave number m varies among the models. The run 4R5 showed the clearest signal of the wave, as we observed a single wave number $m = 5$ persistently propagating with the speed predicted by the slow mode, even without any filtering. However, this run may not capture a realistic wave motion in the Earth's core, where many azimuthal wave numbers will be present. Our lower E runs include more complex drifts generally, and band pass filtering over m is helpful for identifying the wave. We also note that a significant eastward drift was found in the run 6.5R2. However, the speed is much slower than the fast mode, $(\hat{\omega}_{adv} + \hat{\omega}_+)/m$, and cannot simply be explained by the theory we adopted. This necessitates further investigation of wave theories.

4. Discussion

The results suggest that we could use nonaxisymmetric magnetic Rossby waves to infer the strength of the toroidal component of the magnetic field in the Earth's core. The best chance of detection and identification lies with faster propagating high m modes, which travel faster than the core flow. However, the available data is based on geomagnetic observation, where the signals from the core magnetic field are typically limited up to the spherical harmonic degree 12. Nevertheless, the historical geomagnetic model shows a westward drift rate of −0.56°/yr at 40°S, with the dominant wave numbers m of 2, 3, and 5 [*Finlay and Jackson*, 2003]. The estimated angular velocity of the axisymmetric flow has a magnitude of 0.24°/yr westward at the latitude [*Pais et al.*, 2015; private communication, 2015], so the actual speed due to a wave propagation could be about 0.32°/yr. With this speed for an azimuthal wave number $m=5$, the QG model (11) implies a z mean RMS strength $\sqrt{\langle B_\phi^2 \rangle}$ of toroidal field of about 12 mT at $s = 0.77r_\circ$ (see Figure 3). This suggests that the internal toroidal field could be equivalent to or stronger than the 3 mT radial field [*Gillet et al.*, 2010] suggested by torsional oscillation data. This large ratio is present in our numerical simulations, as indicated by a relative strength $B_{T/P}$ of the azimuthal field to the surface radial field (Table 1), although the ratio is less if we compare with the internal radial field at the same radius.

However, we note that this could overestimate the field strength. This is the consequence of the assumption $\xi_z' \approx -(1/s)(\partial u_s'/\partial \phi)$ employed in the theory (section 2). When the radial gradient of the velocity is not negligible, the wave speed goes up; hence, a weaker field is adequate to explain the drift speed. Indeed the geostrophic modes for the Malkus field $\widetilde{\boldsymbol{B}} = B_0 s \hat{\boldsymbol{e}}_\phi$ [*Malkus*, 1967] generally imply faster propagation. Recently, *Canet et al.* [2014] examined the modes in the spherical geometry, assuming several morphologies of
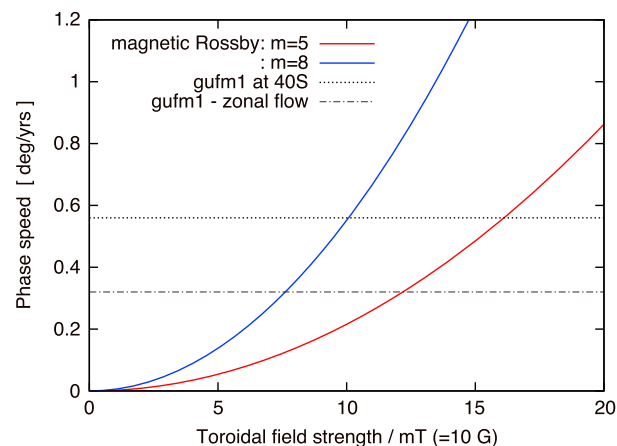
Figure 3. Phase speed of the slow magnetic Rossby wave, $V_{MC} = |\hat{\omega}_{MC}/m|$, versus the z mean strength of axisymmetric toroidal field in the Earth's core. Equation (11) is calculated at $s = 0.77r_\circ$ for wave numbers $m = 5$ and 8, given that $\rho = 1.13 \times 10^4$ kg m^{-3}, $r_\circ = 3.485 \times 10^6$ m, and $\Omega = 7.29 \times 10^{-5}$ s^{-1}. Black dotted and dashed-dotted lines indicate the observed drift speed in the geomagnetic model gufm1 [*Finlay and Jackson*, 2003] and the drift speed where the zonal flow speed obtained in the mean QG flow model inverted from gufm1 over the period 1840–1990 [*Pais et al.*, 2015] is extracted, respectively.

background toroidal field, and found that the field morphologies influenced the radial structure of the modes and the wave speed. However, they also noted that a strong toroidal field was necessary to explain observed wave speeds. A nonaxisymmetric toroidal field will lead to different wave speeds at different longitudes. In contrast to torsional oscillations, where the wave speed measures B_s^2 averaged over geostrophic cylinders, magnetic Rossby waves measure $\boldsymbol{B}^2$ averaged only over z, so the wave speed is a function of s and ϕ, hence of θ and ϕ at the Core-Mantle boundary. More detailed dispersion relations along the lines of, e.g., *Zhang et al.* [2003] and *Schmitt* [2012] would be valuable, but the finding that large toroidal field strengths are needed to explain observed wave speeds is probably robust.

Our simulations suggest that the QG modes may become relevant at higher latitudes, but they are invalid in the vicinity of the equator. Nevertheless, analysis of the Malkus model [*Malkus*, 1967] suggests that equatorial modes will be slow compared to higher-latitude waves. Well-defined waves do exist near the equator [*Jackson*, 2003], but their phase speed is probably dominated by advection due to large-scale flow in the core, as suggested by the models of *Aubert et al.* [2013]. However, the theory could be tested by analyzing the geomagnetic data at higher latitudes over decadal timescales, as indicated by the estimated travel times τ^E (Table 1).

Though the present study focused on free oscillations, which we believe are intrinsic to the core internal dynamics, interactions with the mantle and the solid inner core are probably important to explain the regional differences and permanent features of the geomagnetic westward drift. We also note that stable layers beneath the Core-Mantle boundary could give rise to other wave modes not considered here, which might impact on the secular variation. Different mechanisms for westward drift lead to different dispersion relations: the flow advection with $\omega \propto m$, the magnetic Rossby mode with $\omega \propto m^3$, and, for example, a topographic coupling with a constant drift rate, i.e., ω independent of m [*Yoshida and Hamano*, 1993]. Also, magnetic Rossby waves with a short length scale in the s direction (not evident in these simulations but possibly present in the core) will be affected by the s component of $\widetilde{\boldsymbol{B}}$, which will give a different dispersion relation. It could be possible to evaluate the mechanisms by performing tempo-spatial spectral analyses of the data. The method presented in this study gives a framework for further investigation of the nonaxisymmetric time variation data.

References

Aubert, J., C. C. Finlay, and A. Fournier (2013), Bottom-up control of geomagnetic secular variation by the Earth's inner core, *Nature*, *502*, 219–223.
Bloxham, J., D. Gubbins, and A. Jackson (1989), Geomagnetic secular variation, *Philos. Trans. R. Soc. London, Ser. A*, *329*, 415–502.
Braginsky, S. I. (1970), Torsional magnetohydrodynamic vibrations in the Earth's core and variations in day length, *Geomag. Aeron.*, *10*, 1–8.
Braginsky, S. I. (1999), Dynamics of the stably stratified ocean at the top of the core, *Phys. Earth Planet. Int.*, *111*, 21–34.
Buffett, B. A., J. Mound, and A. Jackson (2009), Inversion of torsional oscillations for the structure and dynamics of Earth's core, *Geophys. J. Int.*, *177*, 878–890.
Buffett, B. A. (2014), Geomagnetic fluctuations reveal stable stratification at the top of the Earth's core, *Nature*, *507*, 484–487.
Bullard, E. C., C. Freedman, H. Gellman, and J. Nixon (1950), The westward drift of the Earth's magnetic field, *Philos. Trans. R. Soc. London, Ser. A*, *243*, 67–92.
Canet, E., C. C. Finlay, and A. Fournier (2014), Hydromagnetic quasi-geostrophic modes in rapidly rotating planetary cores, *Phys. Earth Planet. Int.*, *229*, 1–15.
Christensen, U. R., and P. Olson (2003), Secular variation in numerical geodynamo models with lateral variations of boundary heat flow, *Phys. Earth Planet. Int.*, *138*, 39–54.
Finlay, C. C., and A. Jackson (2003), Equatorially dominated magnetic field change at the surface of Earth's core, *Science*, *300*, 2084–2086.

Finlay, C. C., M. Dumberry, A. Chulliat, and M. A. Pais (2010), Short timescale core dynamics: Theory and observations, *Space Sci. Rev.*, *155*, 177–218.

Gillet, N., and C. A. Jones (2006), The quasi-geostrophic model for rapidly rotating spherical convection outside the tangent cylinder, *J. Fluid Mech.*, *554*, 343–369.

Gillet, N., D. Jault, E. Canet, and A. Fournier (2010), Fast torsional waves and strong magnetic field within the Earth's core, *Nature*, *465*, 74–77.

Hide, R. (1966), Hydromagnetic oscillations of the Earth's core and the theory of the geomagnetic secular variation, *Philos. Trans. R. Soc. London, Ser. A*, *259*, 615–647.

Holme, R., and K. A. Whaler (2001), Steady core flow in an azimuthally drifting reference frame, *Geophys. J. Int.*, *145*, 560–569.

Hori, K., S. Takehiro, and H. Shimizu (2014), Waves and linear stability of magnetoconvection in a rotating cylindrical annulus, *Phys. Earth Planet. Int.*, *236*, 16–35.

Jackson, A. (2003), Intense equatorial flux spots on the surface of the Earth's core, *Nature*, *424*, 760–763.

Jones, C. A. (2007), *Thermal and Compositional Convection in the Outer Core*, vol. 8, edited by G. Schubert, pp. 131–185, Elsevier, Amsterdam.

Kono, M., and P. H. Roberts (2002), Recent geodynamo simulations and observations of the geomagnetic field, *Rev. Geophys.*, *40*(4), 1013.

Malkus, W. V. R. (1967), Hydromagnetic planetary waves, *J. Fluid Mech.*, *28*, 793–802.

Pais, M. A., A. L. Morozova, and N. Schaeffer (2015), Variability modes in core flows inverted from geomagnetic field models, *Geophys. J. Int.*, *200*, 402–420.

Schmitt, D. (2012), Quasi-free-decay magnetic modes in planetary cores, *Geophys. Astrophys. Fluid Dyn.*, *106*, 660–680.

Teed, R. J., C. A. Jones, and S. M. Tobias (2014), The dynamics and excitation of torsional waves in geodynamo simulations, *Geophys. J. Int.*, *196*, 724–735.

Wicht, J., and U. R. Christensen (2010), Torsional oscillations in dynamo simulations, *Geophys. J. Int.*, *181*, 1367–1380.

Yoshida, S., and Y. Hamano (1993), The westward drift of the geomagnetic field caused by length-of-day variation, and the topography of the core-mantle boundary, *Geophys. J. Int.*, *114*, 696–710.

Yukutake, T. (1962), The westward drift of the magnetic field of the Earth, *Bull. Earth. Res. Inst.*, *40*, 1–65.

Zatman, S., and J. Bloxham (1997), Torsional oscillations and the magnetic field within the Earth's core, *Nature*, *388*, 760–763.

Zhang, K., X. Liao, and G. Schubert (2003), Nonaxisymmetric instabilities of a toroidal magnetic field in a rotating sphere, *Astrophys. J.*, *585*, 1124–1137.